Spectroscopic Characterization of Inhibitor Interactions with the Mn(III)/Mn(IV) Core in *Lactobacillus plantarum* Manganese Catalase

Timothy L. Stemmler,[†] Bradley E. Sturgeon,[‡] David W. Randall,[‡] R. David Britt,*[,‡] and James E. Penner-Hahn*[,†]

Contribution from the Department of Chemistry, University of Michigan, Ann Arbor, Michigan 49109, and the Department of Chemistry, University of California, Davis, California 95616

Received February 6, 1997[⊗]

Abstract: X-ray absorption (XAS), UV−visible, electron paramagnetic resonance (EPR), and electron spin echo envelope modulation (ESEEM) spectroscopies have been used to characterize the interaction of azide and cyanide with the Mn(III)(μ-O)$_2$Mn(IV) site in superoxidized Mn catalase. The addition of azide causes no significant change in the X-ray absorption near edge structure (XANES) region and only minor changes in the extended X-ray absorption fine structure (EXAFS) spectra, consistent with only minimal changes in Mn−ligand geometry. In contrast, addition of either azide or cyanide causes an approximately 3-fold increase in the intensity of the visible absorption bands and a small (approximately 4%) decrease in the Mn hyperfine coupling. Anion-binding titrations indicate cooperativity in anion binding. ESEEM experiments on the azide- and cyanide-free enzyme reveal hyperfine ($A = 2.88$ MHz) and electric quadrupolar couplings ($e^2qQ = 2.29$ MHz and $\eta = 0.58$) for a single ^{14}N nucleus of the protein. These parameters are slightly altered upon addition of azide or cyanide, but ESEEM studies with ^{15}N-labeled versions of these inhibitors show that the altered modulation is also due to protein-derived ^{14}N. The ESEEM experiments show no evidence for coupling of azide- or cyanide-derived nitrogens to the Mn cluster. The outer shell scattering in the EXAFS suggests coordination of histidines to the binuclear Mn cluster, and the quadrupolar couplings observed for the protein-derived ESEEM detectable ^{14}N nucleus are consistent with those expected for a histidine imidazole coordinated to Mn(IV). Taken together, these results suggest a model in which azide binds to a protein-derived site, rather than binding directly to either Mn. Despite this indirect binding, azide causes minor perturbations in the Mn$_2$(μ-O)$_2$ geometry, consistent with a slight flattening of the Mn$_2$ core.

Binuclear manganese sites are a common structural theme, with examples including the manganese catalases,[1−3] manganese ribonucleotide reductase,[4] and rat liver arginase.[5] In addition, it has been suggested that the multinuclear Mn cluster in the photosynthetic oxygen evolving complex (OEC) exists as a dimer of Mn$_2$ units.[6] The metal centers in these proteins have been studied extensively using a variety of spectroscopic techniques in order to define the structural, electronic, and reactivity properties of binuclear Mn sites.

The best characterized binuclear Mn center is the active site of the Mn catalases. Manganese catalases catalyze the disproportionation of hydrogen peroxide to oxygen and water. They have been isolated from three bacteria, with the best characterized forms coming from *Lactobacillus plantarum*[7−9] and *Thermus thermophilus*.[3,10] The *L. plantarum* enzyme was found to exist as a hexamer with a subunit weight of 34 000 Da.[7,11] Each subunit contains a binuclear Mn core at the active site.[1] The active enzyme is believed to cycle between the Mn(II)/Mn(II) and Mn(III)/Mn(III) oxidation states.[12] A third oxidation state, the inactive Mn(III)/Mn(IV) form, is also detected in the as-isolated enzyme.[13] The enzyme can be completely converted to the inactive "superoxidized" Mn(III)/Mn(IV) form by treatment with NH_2OH and H_2O_2.[9,12] Superoxidized catalase has a 16-line EPR spectrum at 77 K and is believed to contain a (μ-oxo)$_2$(μ-carboxylato)-bridged Mn(III)/Mn(IV) core.[13] This site shows both structural[14] and spectroscopic[15] similarities to the Mn$_4$ center found in the photosynthetic OEC.

Manganese catalases are inhibited by anions such as N_3^-, CN^-, F^-, and Cl^-, although only at concentrations which are orders of magnitude higher than those needed to inhibit heme catalases.[16−18] Azide is a competitive inhibitor of the *L.*

* Authors to whom correspondence should be addressed.
† University of Michigan.
‡ University of California.
⊗ Abstract published in *Advance ACS Abstracts,* September 15, 1997.

(1) Beyer, W. F. J.; Fridovich, I. *Biochemistry* **1985**, *24*, 6460−6467.
(2) Allgood, G. S.; Perry, J. J. *J. Bacteriol.* **1986**, *168*, 563−567.
(3) Barynin, V. V.; Grebenko, A. I. *Dokl. Akad. Nauk SSSR* **1986**, *286*, 461−464.
(4) Willing, A.; Follmann, H.; Auling, G. *Eur. J. Biochem.* **1988**, *170*, 603−611.
(5) Reczkowski, R. S.; Ash, D. E. *J. Am. Chem. Soc.* **1992**, *114*, 10992−10994.
(6) Debus, R. J. *Biochim. Biophys. Acta* **1992**, *1102*, 269−352.
(7) Kono, Y.; Fridovich, I. *J. Biol. Chem.* **1983**, *258*, 6015−6019.
(8) Kono, Y.; Fridovich, I. *J. Bacteriol.* **1983**, *155*, 742−746.
(9) Kono, Y.; Fridovich, I. *J. Biol. Chem.* **1983**, *258*, 13646−13648.
(10) Vainshtein, B. K.; Melik-Adamyan, W. R.; Barynin, V. V.; Vagin, A. A. In *Progress in Bioorganic Chemistry and Molecular Biology*; Ovchinnikov, Y., Ed.; Elsevier: Amsterdam, New York, and Oxford, 1984; pp 117−132.
(11) Baldwin, E. Thesis, University of North Carolina, Chapel Hill, 1990.
(12) Waldo, G. S.; Fronko, R. M.; Penner-Hahn, J. E. *Biochemistry* **1991**, *30*, 10486−10490.
(13) Fronko, R. M.; Penner-Hahn, J. E.; Bender, C. J. *J. Am. Chem. Soc.* **1988**, *110*, 7554−7555.
(14) Waldo, G. S.; Yu, S.; Penner-Hahn, J. E. *J. Am. Chem. Soc.* **1992**, *114*, 5869−5870.
(15) Dismukes, G. C.; Tang, X. S.; Khangulov, S. V.; Sivaraja, M.; Pessiki, P. In *Research Photosynthesis*; Murata, N., Ed.; Kluwer: Dordrecht, 1992; Vol. 2, pp 257−264.
(16) Penner-Hahn, J. E. In *Manganese Redox Enzymes*; Pecoraro, V. L., Ed.; VCH Publishers, Inc.: New York, 1992; pp 29−45.
(17) Khangulov, S. V.; Goldfeld, M. G.; Gerasimenko, V. V.; Andreeva, N. E.; Barynin, V. V.; Grebenko, A. I. *J. Inorg. Biochem.* **1990**, *40*, 279−292.

S0002-7863(97)00404-6 CCC: $14.00

Table 1. XAS Data Collection and Reduction Parameters

	sample 1 ± azide	sample 2 ± azide	sample 3[a]
beamline	SSRL, VII-3	NSLS, X-9A	NSLS, X-19A
monochromator crystal	Si[220]	Si[220]	Si[111]
cryostat type	Oxford He flow	Displex cold-finger	Oxford He flow
scan length (min)	40	35	36
scans in average	12, 14	9, 9	9
Mn concentration (mM)	3.6	4.0	5.0
temperature (K)	10	40	12
beam size (mm^2)	1.5 × 9	2 × 10	2 × 10
pre-edge region (polynomial order)	6310−6520 (−2)	6310−6520 (−2)	6340−6520 (−2)
spline regions (polynomial order)	6567−6680 (2)	6567−6680 (2)	6565−6680 (2)
	6680−6850 (3)	6680−6850 (3)	6680−6850 (3)
	6850−7200 (3)	6850−7200 (3)	6850−7100 (3)

[a] No azide-bound data were measured for this sample.

plantarum enzyme, with an inhibition constant (K_i) of 80 mM at 25 °C and pH 7.0.[16] Although the superoxidized Mn catalase is inactive, it is nevertheless sensitive to the presence of azide and cyanide. This was originally noted as a perturbation in the 16-line EPR spectrum upon addition of azide to the *L. plantarum* enzyme.[16] More recently, azide has been shown to perturb the magnetic circular dichroism (MCD) spectrum of superoxidized catalase.[19]

In the present paper, we describe a detailed spectroscopic investigation of ion binding to the superoxidized form of the *L. plantarum* Mn catalase. Azide and cyanide have frontier molecular orbitals similar to those in H_2O_2; thus insight into the interactions of these two ions with catalase may give information about peroxide binding to the active enzyme. Moreover, given the structural (i.e., EXAFS) similarities between Mn(III)/Mn(IV) catalase and the Mn cluster of the OEC, a more detailed understanding of anion interactions with the Mn catalase may be helpful in understanding the more complex Mn site(s) in the OEC.

Experimental Procedures

Sample Purification and Preparation. Manganese catalase was isolated from *L. plantarum* using a modification of the published protocol[7] in which batchwise DE-52 extraction followed by chromatography was replaced by a single fast-flow DEAE Sepharose column. Additional purification was accomplished using a G-150 Sephadex size exclusion column. Enzyme activity was assayed using a Clark-type oxygen electrode (YSI 5331). Protein concentration was determined relative to A_{280}/A_{260}.[20] Specific activities were between 3000 and 3600 AU/mg (1 activity unit (AU) = decomposition of 1 μmol of H_2O_2/min, with $[H_2O_2] = 0.02$ M). Superoxidized samples were prepared according to the following three-step protocol: (1) 12-hour aerobic dialysis against a 50 mM H_2O_2/20 mM NH_2OH solution in 50 mM sodium phosphate buffer ($T = 4$ °C, pH 7.0); (2) 12-h aerobic dialysis in a 50 mM H_2O_2 solution with 50 mM sodium phosphate buffer ($T =$ 4 °C, pH 7.0); and (3) 12-h aerobic dialysis in 50 mM sodium phosphate buffer ($T = 4$ °C, pH 7.0). Samples were concentrated using Amicon-50 concentrators.

XAS samples were prepared at pH 7.0 in 50 mM sodium phosphate buffer. Azide samples were prepared by incubating superoxidized enzyme in ca. 200 mM N_3^- solutions. Three independent samples of azide-free catalase and two independent azide-treated samples were prepared under identical conditions by first concentrating the enzyme solutions and then diluting them to a final Mn concentration of ca. 4.5 mM with glycerol to a final glycerol concentration of 40%. The enzyme solutions were injected into Lucite cells which were covered with 6 μm polypropylene film.

Enzyme samples for EPR, ESEEM, and UV−visible studies were prepared in 50 mM sodium phosphate buffer (pH 7.0) at Mn concentrations of 0.23, 0.48, and 1.7 mM, respectively. EPR samples in 50 mM MES (pH 5.5), 50 mM HEPES (pH 7.0), and 50 mM TRIS (pH 8.5) were prepared using biograde buffers purchased from Sigma Chemical Co. Samples for the spectroscopic titrations were prepared by injecting the appropriate volume of a concentrated (1.5 M) solution of buffered NaN_3 or NaCN directly into the enzyme solution, followed immediately by mixing for 2 min. Isotopically labeled $Na^{15}NNN$ and $NaC^{15}N$ were purchased from Cambridge Isotope Laboratories, and labeled catalase samples were prepared in the same way as the unlabeled samples.

XAS Data Collection and Analysis. Manganese K-edge XAS measurements were performed both at the Stanford Synchrotron Radiation Laboratory (SSRL) and at the National Synchrotron Light Source (NSLS) at Brookhaven National Laboratory. Data were measured as fluorescence excitation spectra using a 13-element Ge solid state detector. Both facilities were operating under dedicated conditions (3.0 GeV/100 mA and 2.5 GeV/200 mA, respectively). Details of the data collection and reduction are given in Table 1. XAS spectra were averaged independently for each data set collected at each location. Monochromator energies were calibrated relative to the energy of the pre-edge peak in a $KMnO_4$ standard, defined as 6543.3 eV. Average files were calculated using all three EXAFS data sets for the azide/cyanide-free enzyme and both data sets for the azide-bound enzyme. EXAFS data reduction followed standard procedures for pre-edge subtraction and spline background removal.[21] Once data were converted from eV to k space, Fourier transforms for all spectra were calculated using k^3 weighted data from 1.5 to 12.0 $Å^{-1}$. Initial fits were performed on Fourier-filtered data which were backtransformed over $R = 1.4$−4.3 Å to eliminate high-frequency noise. Subsequent curve fitting using unfiltered data gave identical structural results.

Absorber−scatterer information was obtained from fitting the EXAFS data to eq 1,

$$\chi(k) = \sum_S \frac{N_s A_s(k) S}{k R_{as}^2} \exp(-2k^2\sigma_{as}^2) \sin(2kR_{as} + \phi_{as}(k)) \quad (1)$$

where $\chi(k)$ is the fractional modulation in the absorption coefficient above the edge, N_s is the number of scatterers at a distance R_{as}, $A_s(k)$ is the effective backscattering amplitude, S is a scale factor, σ_{as}^2 is the mean-square deviation in R_{as}, ϕ_{as} is the phase-shift that the photoelectron wave undergoes in passing through the potentials of the absorbing and scattering atoms, and the sum is taken over all shells of scatterers. Theoretical models for the EXAFS amplitude and phase functions were calculated using the program FEFF 5.04.[22] The FEFF parameters were calibrated using a multiplicative scale factor and an adjustable E_0 that were determined by fitting EXAFS data for crystallographically characterized Mn models.[23,24] An E_0 value of 10 eV and a scale factor

(18) Waldo, G. S. Ph.D. Thesis, The University of Michigan, 1991.
(19) Gamelin, D. R.; Kirk, M. L.; Stemmler, T. L.; Pal, S.; Armstrong, W. H.; Penner-Hahn, J. E.; Solomon, E. I. *J. Am. Chem. Soc.* **1994**, *116*, 2392−2399.
(20) Warburg, O.; Christian, W. *Biochem. Z.* **1942**, *310*, 384−421.
(21) Scott, R. A. *Methods Enzymol.* **1985**, *117*, 414−459.
(22) Rehr, J. J.; Mustre, D. L. J.; Zabinsky, S. I.; Albers, R. C. *J. Am. Chem. Soc.* **1991**, *113*, 5135−5140.
(23) Riggs-Gelasco, P. J.; Stemmler, T. L.; Gelasco, A. K.; Kitajima, N.; Pecoraro, V. L.; Penner-Hahn, J. E., unpublished results.

of 0.9 were used to fit the <3 Å scattering, while an E_0 of 6.0 and a scale factor of 0.75 were used to fit the >3 Å scattering. Theoretical models were calculated for single scattering Mn−O, Mn−N, and Mn···Mn interactions at bond lengths of 1.82, 2.14, and 2.70 Å, respectively. Theoretical models incorporating multiple scattering interactions were calculated for the ca. 3.2 Å Mn···C_2/C_5 and ca. 4.4 Mn···N_3/C_4 imidazole interactions. The outer shell Mn···C and Mn···N models were calibrated by fitting EXAFS data for hexakisimidazole Mn(II) dichloride.[25]

Nonlinear least-squares curve fitting was used to optimize Mn−ligand distances and coordination numbers. In all cases, only R and σ were allowed to vary, while the coordination number was held constant at a series of chemically reasonable half-integer values. The root-mean-square deviation between data and fit (F'), weighted by the number of degrees of freedom, was calculated for all fits to Fourier-filtered data.[26] The F' parameter, weighted with respect to the number of free variables in the data, introduces a penalty for adding additional unnecessary shells of scatterers and thus provides a more reliable basis for deciding whether an additional shell is justified.[27]

XANES spectra were normalized by fitting the data both below and above the edge to tabulated X-ray absorption cross sections using a single second-order polynomial and a single scale factor.[18,28] Areas for the 1s → 3d pre-edge transitions were calculated by first fitting an arctangent background to the normalized data below (6530−6538 eV) and above (6543.5−6550 eV) the 1s → 3d transition. The normalized area of the pre-edge peak after background subtraction was obtained by numerical integration over the range 6538 to 6543.5 eV and is expressed in units of 10^{-2} eV.[29] Normalized protein 1s → 3d areas were compared to those obtained for four Mn(III/IV) models: {Mn^{III}/Mn^{IV}(1,3-bis((3,5-Cl_2(1,3-(salicyliden)amino)-2-propanol)$_2$}ClO_4 (**A**);[30] {Mn^{III}/Mn^{IV}(1,3-bis(3,5-Cl_2-salicylidene)amino)-2-propanol)$_2$-(THF)}$^+$ (**B**);[31] {Mn^{III}/Mn^{IV}((hydrotris(3,5-diisopropyl-1-pyrazolyl)-borate)$_3$)$_2$}$(O)_2(OAc)$ (**C**);[32] and {$Mn^{III}/Mn^{IV}(O)_2$(2,2′-bipyridine)$_2$} (**D**).[33] Each model has two six-coordinate Mn ions, with either monoalkoxo or bisoxo bridges. Low-temperature (10 K) XAS spectra[23,34] for these models were analyzed in the same way as the protein data.

UV−Visible Spectroscopy. UV−visible spectra were measured using a dual beam Shimadzu UV 2101-PC instrument. Measurements were made at room temperature using 500 μL quartz cuvettes with a path length of 1 cm.

EPR Spectroscopy. EPR spectra were measured using a Bruker ER 200E-SRC EPR spectrometer with a modified console, equipped with a TM(110) cavity operating at ca. 9.5 GHz. The spectrometer was interfaced with a Samsung personal computer, and data were digitized using EWSin software from Scientific Software Services. All measurements were made at 77 K using 20 mW microwave power, 0.5 mT peak-to-peak modulation amplitude, and 100 kHz modulation frequency. Under these conditions, the signals were not saturated.

EPR Simulations. EPR data were simulated using a nonlinear least-squares optimization of a third-order perturbation expression.[35] Simulations were run on a VAX station 4000/60.

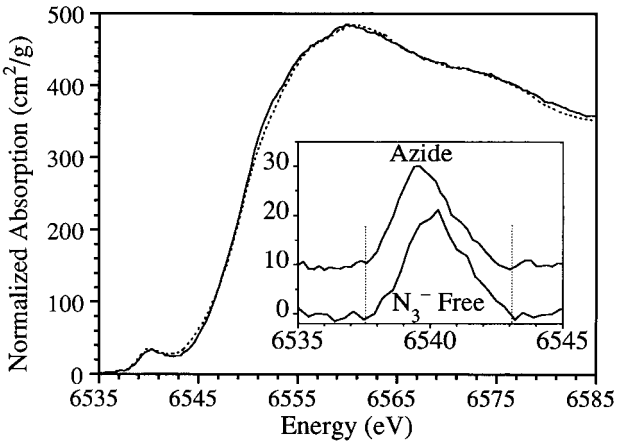

Figure 1. Normalized XANES spectra of azide-free superoxidized catalase (solid line) and superoxidized catalase + azide (dashed line). Inset: Background-subtracted 1s → 3d transitions. As a guide to the eye, the approximate extent of the 1s → 3d region is indicated by the vertical dashed lines.

Titration Curve Analysis. Titration curves were determined from both the UV−visible and EPR titration data. The fraction of enzyme with the anion bound, θ, was determined by fitting each spectrum (corrected for dilution) with linear combinations of the extreme spectra, measured in the absence of anions and at the maximum anion concentration. The data for θ as a function of anion concentration, [I], show evidence for cooperative binding (see below) and could be fit to a variety of equilibrium binding models (see Supporting Information). The strength of the anion binding was characterized by the anion concentration giving $\theta = 0.5$, $[I]_{1/2}$.

ESEEM Spectroscopy. The ESEEM experiments were performed with a laboratory-built pulsed EPR spectrometer.[36] X-band (8−12 GHz) experiments were performed with a loop-gap resonator probe structure with samples loaded into 3.8 mm o.d. quartz tubes.[37] P-band (12−18 GHz) experiments were performed with a high-frequency version of the Mims stripline cavity with samples loaded directly into a Teflon well surrounding the stripline element.[38] All experiments were performed at a temperature of 4.2 K using a 3-pulse ESEEM sequence.[39]

X- and P-band ESEEM spectra were collected on samples of superoxidized catalase ± azide and ± cyanide. P-band spectra were collected for Mn(III)/Mn(IV) catalase ± azide samples using the following values for the microwave frequencies (ν_{MW}), magnetic fields (B), and interpulse times (τ): $\nu_{MW} = 13.098$ GHz (N_3^--free enzyme), 12.980 GHz (NNN^-), and 13.206 GHz ($^{15}NNN^-$); $B = 477.1$ mT (N_3^--free enzyme), 474.8 mT (NNN^-), and 483.5 mT ($^{15}NNN^-$); and $\tau =$ 197 ns (N_3^--free enzyme), 200 ns (NNN^-), and 196 ns ($^{15}NNN^-$). All X-band ESEEM spectra were collected using the following parameters: $\nu_{MW} = 10.995$ GHz; $B = 400.2$ mT; $\tau = 176$ ns, respectively. P-band spectra were collected for Mn(III)/Mn(IV) catalase ± cyanide samples using the identical values for ν_{MW}, B, and τ of 13.718 GHz, 528.9 mT, and 222 ns, respectively, while X-band data were collected for these samples at 9.2774 GHz, 331.1 mT, and 213 ns. Additional parameters used in all data collection were a repetition rate of 200 Hz, a $\pi/2$ pulse width of 15 ns, and a microwave power of ca. 10 W. ESEEM simulations were performed as previously described[40] using the matrix diagonalization protocol described by Mims.[41]

Results

XAS Spectroscopy. XANES spectra for Mn(III)/Mn(IV) catalase ± azide are shown in Figure 1. Both the shapes and

(24) Stemmler, T. L.; Sossong, T. M., Jr.; Goldstein, J. I.; Ash, D. E.; Elgren, T. E.; Kurtz, D. M., Jr.; Penner-Hahn, J. E. *Biochemistry* **1997**, *36*, 9847−9858.
(25) Garrett, T. P. J.; Guss, J. M.; Freeman, H. C. *Acta Crystallogr. Sect. C: Cryst. Struct. Commun.* **1983**, *39*, 1027−1031.
(26) Riggs-Gelasco, P. J.; Mei, R.; Yocum, C. F.; Penner-Hahn, J. E. *J. Am. Chem. Soc.* **1996**, *118*, 2387−2399.
(27) Riggs-Gelasco, P. J.; Stemmler, T. L.; Penner-Hahn, J. E. *Coord. Chem. Rev.* **1995**, *144*, 245−286.
(28) McMaster, W. H.; Del Grande, N. K.; Mallett, J. H.; Hubbel, J. H. "Compilation of X-Ray Cross Sections"; U.S. Department of Commerce, 1969.
(29) Roe, A. L.; Schneider, D. J.; Mayer, R. J.; Pyrz, J. W.; Wisdom, J.; Que, J. L. *J. Am. Chem. Soc.* **1984**, *106*, 1676−1681.
(30) Gelasco, A. K. Ph.D. Thesis, The University of Michigan, 1995.
(31) Larson, E. J.; Haddy, A.; Kirk, M. L.; Pecoraro, V. L. *J. Am. Chem. Soc.* **1992**, *114*, 6263−6265.
(32) Kitajima, N., personal communication.
(33) Plaskin, P. M.; Stoufer, R. C.; Mathew, M.; Palenik, G. J. *J. Am. Chem. Soc.* **1972**, *94*, 2121−2122.
(34) Riggs-Gelasco, P. J. Thesis, The University of Michigan, 1995.
(35) Haddy, A.; Waldo, G. S.; Sands, R. H.; Penner-Hahn, J. E. *Inorg. Chem.* **1994**, *33*, 2677−2682.
(36) Sturgeon, B. E.; Britt, R. D. *Rev. Sci. Instrum.* **1992**, *63*, 2187−92.
(37) Britt, R. D.; Klein, M. P. *J. Magn. Reson.* **1987**, *74*, 535−540.
(38) Sturgeon, B. E.; Ball, J. A.; Randall, D. W.; Britt, R. D. *J. Phys. Chem.* **1994**, *98*, 12871−12883.
(39) Britt, R. D. In *Biophysical Techniques in Photosynthesis*; Amesz, J. Hoff, A. J., eds.; Kluwer Academic: Dordrecht, 1996; pp 235−253.
(40) Britt, R. D.; Zimmermann, J. L.; Sauer, K.; Klein, M. P. *J. Am. Chem. Soc* **1989**, *111*, 3522−3532.
(41) Mims, W. B. *Phys. Rev. B* **1972**, *5*, 2409−2419.

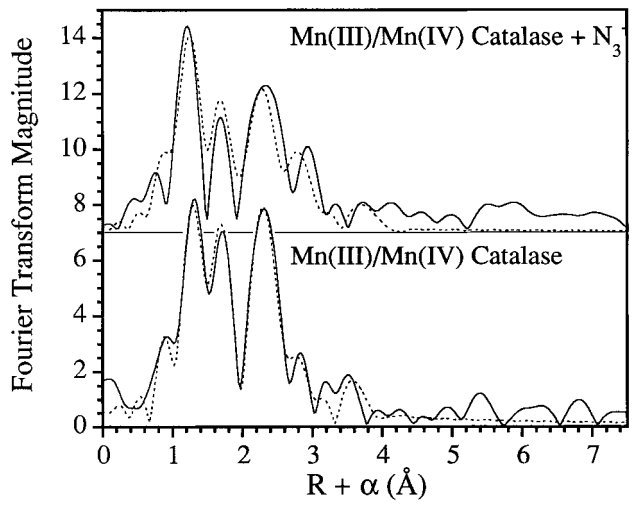

Figure 2. Fourier transforms of the EXAFS data for superoxidized catalase ± azide. Top: with azide. Bottom: without azide. For each plot, the solid line is the average of experimental data, the dashed line is the best fit.

energies of these spectra are virtually identical. The first inflection point of the edge occurs at 6549.2 eV for both spectra; this is consistent with the edge energies of Mn(III) and Mn(IV) model XANES spectra.[23] The average 1s → 3d area for the azide-free Mn(III)/Mn(IV) catalase spectra was 14.5 (±0.4) × 10^{-2} eV, while that for the azide-bound spectra was 14.6 (±1.2) × 10^{-2} eV. These values are within the range of the areas seen for the Mn(III)/Mn(IV) models. The two non-oxo-bridged models have smaller areas, 8.0 × 10^{-2} eV (**A**) and 6.0 × 10^{-2} eV (**B**), while the two μ-oxo-bridged models have larger areas, 15.8 × 10^{-2} eV (**C**) and 25.6 × 10^{-2} eV (**D**).

The 1s → 3d transition consists of several unresolved transitions.[42] Although the range of energies covered by the unresolved 1s → 3d transitions is not affected by the addition of azide (see inset to Figure 1), the distribution of intensity within the transition manifold changes slightly when azide binds. The slight increase in the relative contribution of the lower energy transitions in the presence of azide probably reflects a small change in the Mn electronic structure.

Fourier transforms of the averaged data for the Mn(III)/Mn(IV) catalase ± azide samples are shown in Figure 2. Both samples show a well-resolved feature at $R + \alpha \approx 1.3$ Å, which is characteristic of short metal−oxo bonds. A second feature is apparent in both spectra at $R + \alpha \approx 1.7$ Å. This is attributable to a second resolvable shell of Mn−nearest neighbor scatters. A dominant feature in both spectra is a peak at $R + \alpha \approx 2.4$ Å. This is characteristic of the Mn···Mn scattering found in di(μ-oxo)-bridged Mn(III)/Mn(IV) cores.[14] Both spectra also show long-range features at $R + \alpha > 3.0$ Å which are characteristic of the Mn···(N_3/C_4) interactions seen in Mn−imidazole models.[24]

Although both samples have the same four principal peaks, the relative intensities and apparent resolution of these peaks are different. This reflects one of the difficulties of Fourier transform analysis, since minor variations in individual bond lengths can cause significant changes in the Fourier transforms due to changes in interference. For this reason, all structural conclusions are based on *k*-space curve-fitting analyses.

Table 2 summarizes the curve-fitting results for all of the azide-free and -bound superoxidized catalase XAS samples. Results are given for fits to both Fourier-filtered and -unfiltered averaged data and for fits to the unfiltered individual files. In all cases, three dominant shells of scatterers account for most of the features of the data. These results are typical of those seen for other high-valent binuclear metalloproteins with a short M−O_{oxo} shell at ca. 1.8 Å with a second shell of low Z scatterers at a longer distance.[23] The addition of a Mn···Mn shell causes a large reduction in F', indicating that the Mn···Mn scattering is a large component in the overall scattering in every sample. Although the Mn···Mn feature in the Fourier transform of the azide spectrum appears distorted, attempts to fit this feature with an additional shell of Mn···N at ca. 2.8 Å (the approximate distance expected for the β-nitrogen from an end-on bound azide) were unsuccessful. The Mn···Mn distances in Table 2 are slightly longer than those reported previously for azide-free catalase.[14] This is most likely the result of improved phase calibration in the present study.[43] The observed Mn···Mn distances are characteristic of those found in di(μ-oxo)-bridged Mn dimers.[44]

For the average data, there is a small increase in both N_s and σ_{as}^2 for the Mn−O/N shell when azide binds. Given the uncertainty of EXAFS for measuring coordination numbers (±0.5) and the correlation between N_s and σ_{as}^2, this difference is likely to reflect only fitting errors. In contrast, there is a larger, reproducible increase in σ_{as}^2 for the Mn−O_{oxo} shell on azide addition, suggesting increased disorder in the Mn_2O_2 core structure. Finally, there are small but reproducible changes in the Mn−O/N and Mn···Mn distances on binding of azide. On the basis of the reproducibility between data sets, the precision in determining the Mn−O_{oxo}, Mn−O/N, and Mn···Mn bond lengths is ∼0.005 Å. Since the apparent bond length depends on E_0, variations in E_0 can complicate attempts to determine *R*. However, E_0 was held fixed, and moreover, there should be no significant change in E_0 since there is no change in the edge energies. Therefore, the changes in the apparent bond lengths are likely to represent real structural changes. These minor changes in bond lengths will cause small changes in intershell interference and thus can account for the changes in size and shape of the Fourier transform features.

For all samples, there are additional minor features in the Fourier transforms at higher *R* ($R + \alpha \approx 2.6$−4.0 Å). These are typical of the outer shell peaks that are seen for imidazole ligation.[45,46] The outer shell scattering was modeled using multiple scattering parameters for Mn−imidazole ligation.[24] The data could be fit using both 3.0 and 4.3 Å Mn···C shells. For all samples except the untreated sample **2**, the fit quality (F') improved for the 5-shell fit vs the 3-shell fit (compare fits F and C). Inclusion of the 4.3 Å carbon shell generally gave improved fits in comparison with the 3-shell fits (compare fits E and C), but did not typically result in an improvement (decreased F') in comparison to the 4-shell fits (compare fits F and D). This reflects the fact that the 4.3 Å carbon shell, while well defined in terms of distance, makes only a very small contribution to the overall EXAFS. In comparing fits F and D, the small decrease in the mean-square-deviation that results from inclusion of the 4.3 Å carbon shell is not sufficient to offset the decrease in the number of degrees of freedom from ca. 11 to 9. The carbon scattering at ca. 4.3 Å is at the distance expected for the N_3/C_4 scattering from Mn(III)- and Mn(IV)−

(42) Westre, T. E.; Kennepohl, P.; DeWitt, J. G.; Hedman, B.; Hodgson, K. O.; Solomon, E. I. *J. Am. Chem. Soc.* **1997**, *119*, 6297−6314.

(43) The differences in Mn···Mn distance are not due to differences between samples, as confirmed by reanalysis of the previous data (entry **3** in Table 2).

(44) Larson, E.; Lah, M. S.; Li, X.; Bonadies, J. A.; Pecoraro, V. L. *Inorg. Chem.* **1992**, *31*, 373−378.

(45) Wang, S.; Lee, M. H.; Hausinger, R. P.; Clark, P. A.; Wilcox, D. E.; Scott, R. A. *Inorg. Chem* **1994**, *33*, 1589−1593.

(46) Strange, R. W.; Hasnain, S. S.; Blackburn, N. J.; Knowles, P. F. *J. Phys., Colloq.* **1986**, *C8* (2), 593−596.

Table 2. XAS Curve Fitting Results[a] and 1s → 3d Areas

		Mn−O_{oxo}			Mn−O/N			Mn···Mn			Mn···C			Mn···C				
sample	fit	R_{as}	N_s	σ_{as}^2	R_{as}	N_s	σ_{as}^2	R_{as}	N_s	σ_{as}^2	R_{as}	N_s	σ_{as}^2	R_{as}	N_s	σ_{as}^2	F' [b]	1s → 3d[c]
avg[d]	A	1.81	2.0	2.2													11.6	
	B	1.82	2.0	0.9	2.07	2.5	4.4										8.59	
	C	1.82	2.0	1.9	2.09	2.5	4.5	2.69	1.0	2.2							1.68	
	D	1.82	2.0	1.9	2.09	2.5	5.0	2.70	1.0	1.8	2.95	3.5	3.1				1.52	
	E	1.82	2.0	1.9	2.09	2.5	5.0	2.70	1.0	2.6				4.31	2.5	1.3	1.65	
	F	*1.82*	*2.0*	*1.9*	*2.09*	*2.5*	*5.0*	*2.70*	*1.0*	*1.8*	*2.95*	*3.5*	*3.1*	*4.31*	*2.5*	*3.7*	1.59	
	F	1.82	2.0	1.8	2.08	2.5	5.8	2.70	1.0	2.0	2.96	3.5	3.2	4.31	2.5	3.0		
1[e]	F	*1.81*	*2.0*	*4.0*	*2.10*	*3.0*	*5.4*	*2.70*	*1.0*	*3.2*	*3.00*	*5.5*	*1.0*	*4.28*	*2.5*	*3.7*		14.5
2[e]	F	*1.82*	*2.0*	*1.8*	*2.09*	*2.5*	*4.2*	*2.69*	*1.0*	*3.1*	*2.97*	*4.0*	*3.6*	*4.31*	*3.0*	*1.7*		14.8
3[e,f]	F	*1.82*	*2.0*	*1.3*	*2.11*	*2.5*	*8.1*	*2.69*	*1.0*	*2.3*	*2.94*	*3.5*	*7.0*	*4.31*	*2.0*	*3.8*		14.7
avg[d] + N_3^-	A	1.84	2.0	11.2													9.42	
	B	1.81	2.0	2.8	2.05	3.0	5.5										6.62	
	C	1.81	2.0	3.6	2.05	3.0	6.5	2.72	1.0	3.1							1.91	
	D	1.81	2.0	3.5	2.05	3.0	6.5	2.73	1.0	3.0	3.00	4.0	0.9				1.25	
	E	1.81	2.0	3.5	2.05	3.0	6.5	2.72	1.0	1.7				4.34	1.0	1.3	1.69	
	F	1.81	2.0	3.6	2.05	3.0	6.5	2.73	1.0	3.0	3.00	4.0	0.9	4.33	1.0	3.0	1.43	
	F	*1.81*	*2.0*	*3.1*	*2.04*	*3.0*	*6.4*	*2.73*	*1.0*	*3.0*	*3.00*	*4.0*	*1.0*	*4.34*	*1.5*	*3.1*		
1 + N_3^- [e]	F	*1.80*	*2.0*	*3.1*	*2.03*	*2.5*	*5.6*	*2.73*	*1.0*	*4.0*	*3.00*	*5.0*	*1.7*	*4.36*	*1.0*	*4.2*		13.7
2 + N_3^- [e]	F	*1.81*	*2.0*	*3.6*	*2.05*	*2.5*	*4.9*	*2.73*	*1.0*	*2.9*	*2.99*	*3.5*	*2.7*	*4.29*	*1.5*	*2.0*		15.4

[a] Values in italics were obtained from fits to unfiltered data. R_{as} = Mn−scatterer distance in Å; N_s = coordination number per Mn; σ_{as}^2 = Debye−Waller factor in units of Å × 10^{-3}. [b] F' is a weighted goodness of fit parameter × 10^{-2}. [c] Normalized areas given in ×10^{-2} eV units. [d] Average data, Fourier filtered over the range of R = 1.4−4.3 Å. [e] Best fit to unfiltered individual data sets. [f] Sample was previously reported[14] with slightly different fitting results (see text).

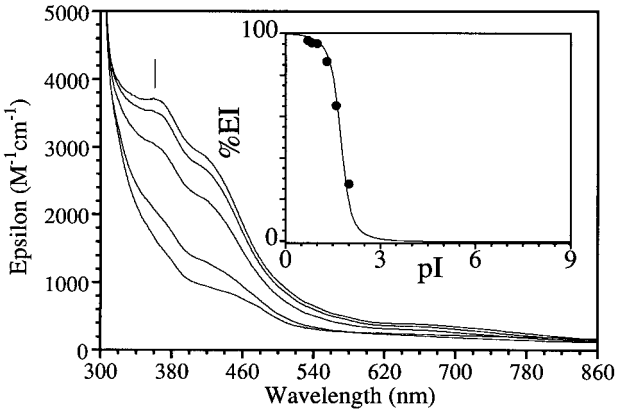

Figure 3. UV−Vis spectra for superoxidized catalase in the presence of azide. Titration at azide concentrations of 232, 50.3, 25.3, 10.0, and 0.0 mM, from top to bottom at 362 nm. Inset shows the percent EI vs pI (see text), together with the best fit to a two-site allosteric model. All spectra were measured at 25 °C and have been corrected for dilution.

imidazole interactions. The apparent amplitude of 1.5−2.5 carbons per Mn is consistent with the presence of one imidazole ligand per Mn. Fourier transforms simulated from the best fit 5-shell fits are compared to the empirical spectra in Figure 2.

UV−Visible Spectroscopy. The absorption spectra as a function of the azide concentration are shown in Figure 3. The dominant features in the superoxidized catalase spectrum are peaks at 362 and 442 nm, with a weak feature at 621 nm.[19] Addition of azide to the Mn(III)/Mn(IV) enzyme causes an increase in the intensity of all of these features for azide concentrations <100 mM. Higher azide concentrations (to 232 mM N_3^-) caused no additional changes in the UV−visible spectrum. On the basis of these data, the $[N_3^-]_{1/2}$ is 18 mM at 25 °C, pH 7.0. The binding curve (inset to Figure 3) demonstrates that conversion from mostly azide-free to mostly azide-bound form is complete over less than a 10-fold change in $[N_3^-]$. This is inconsistent with simple binding of azide to six noninteracting sites for the hexanuclear Mn catalase. A variety of cooperative binding models can be used to fit the data (see Supporting Information). The best fit using a two-state allosteric model is shown in the inset to Figure 3.

Qualitatively similar spectral changes are observed on addition of cyanide to superoxidized catalase (data not shown). In this case, however, cyanide concentrations >110 mM caused protein precipitation, and thus it was possible to obtain only a lower limit of the affinity for cyanide at pH 7.0. Using the cyanide-free and the 110 mM cyanide spectra as the lower and upper limit spectra, respectively, a lower limit for $[CN^-]_{1/2}$ is ∼50 mM at 25 °C, pH 7.0.

EPR Spectroscopy. Initial measurements of the effects of azide and cyanide on the EPR spectrum suggested significantly tighter anion binding than was found in the UV−visible titrations. This was ultimately traced to the use of sodium phosphate buffer and is attributed to a change in pH on freezing.[47] Subsequent measurements were made using HEPES (pH 7.0) and MES (pH 5.5) to avoid this effect. The X-band EPR spectra of superoxidized catalase as a function of azide concentration at pH 7.0 and 77 K are shown in Figure 4. Spectra were measured at 15 different azide concentrations up to 242 mM and are compared to the spectrum for the superoxidized enzyme in the absence of azide. Spectra measured at azide concentrations >101 mM were identical. Addition of azide causes a decrease in the overall hyperfine splitting, along with subtle changes in some of the line shapes. Vertical lines mark the position of the low- and high-field features in the absence of azide. Linear combinations of the limiting spectra were used to fit the spectra for intermediate azide concentrations. The best fits (not shown) were obtained for 30:70 (26.3 mM) and 69:31 (68.7 mM) ratios of azide-free and azide-saturated spectra. Hill plots (supplementary material) give a Hill coefficient of approximately 2.5, providing further evidence for a cooperative binding interaction. The apparent $[N_3^-]_{1/2}$ is 40 mM at 77 K ($pH_{25°C}$ 7.0). The azide-induced perturbations of the multiline EPR spectrum were reversed by dialysis (12 h) against azide-free buffer.

The ability of azide to perturb the EPR spectrum is strongly dependent on pH. Additional measurements were made for the superoxidized enzyme at pH 5.5 and 8.5. At pH 8.5, the addition of up to 150 mM azide did not cause any detectable

(47) Hill, J. P.; Buckley, P. D. *Anal. Biochem.* **1991**, *192*, 358−361.

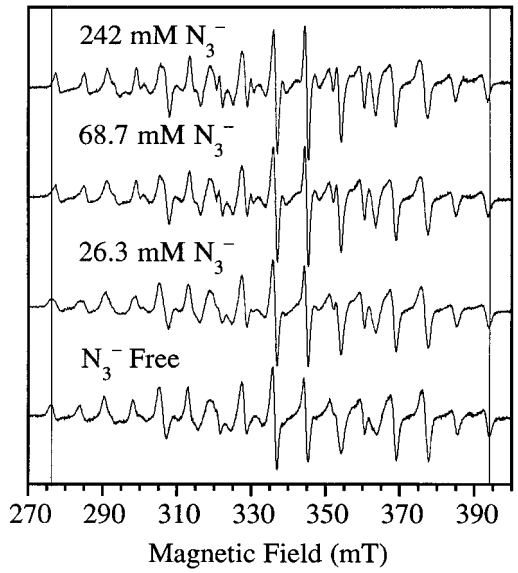

Figure 4. X-band EPR titration of Mn(III)/Mn(IV) catalase with azide at pH 7.0 in HEPES. [N_3^-] (top to bottom) = 242, 68.7, 26.3, and 0.0 mM, offset for clarity. Vertical lines mark 276.3 and 393.7 mT. Temperature was 77 K.

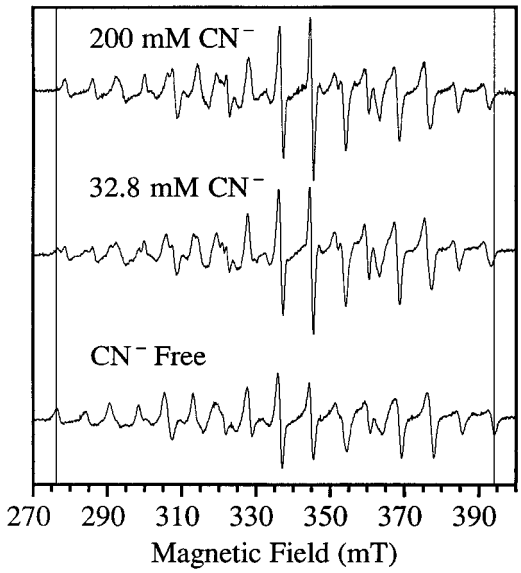

Figure 5. X-band EPR titration of Mn(III)/Mn(IV) catalase with cyanide at pH = 5.5 in MES. [CN^-] (top to bottom) = 200, 32.8, and 0.0 mM, offset for clarity. Vertical lines mark 276.3 and 393.7 mT. Temperature was 77 K.

changes in the EPR spectrum. In contrast, the titration at pH 5.5 gave an apparent $[N_3^-]_{1/2}$ of 5.0 mM at 77 K (data not shown).

Addition of cyanide to the superoxidized catalase causes changes in the EPR spectrum that are similar to those seen for the azide addition, although higher cyanide concentrations (ca. 100 mM, pH 5.5) were required for complete conversion. Representative spectra from the EPR-detected-cyanide titration of superoxidized catalase at pH 5.5 in MES are shown in Figure 5. The intermediate spectrum in Figure 5 was best fit (not shown) with a 61:39 ratio of the extreme spectra. The fitting results for the cyanide titrations (supplementary material) are very similar to those for azide, with the apparent $[CN^-]_{1/2}$ = 28 mM at 77 K ($pH_{25°C}$ 5.5). As with azide, cyanide could be removed by dialysis to regenerate the original EPR spectrum. In addition to azide and cyanide, fluoride is also an inhibitor of

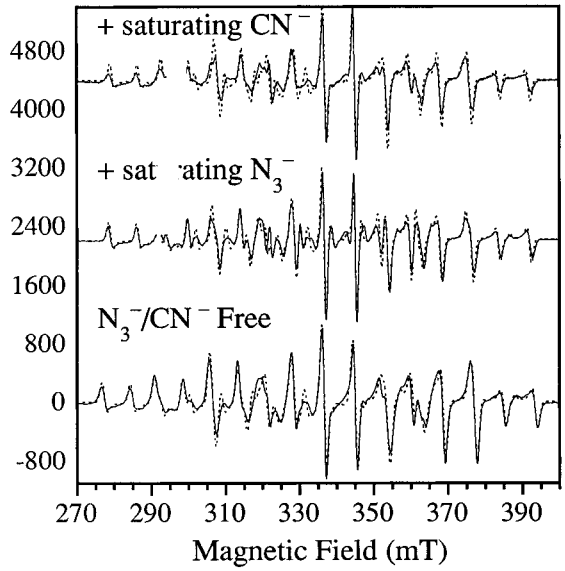

Figure 6. X-band EPR spectra (solid lines) and simulations (dash lines) for Mn(III)/Mn(IV) catalase + saturating (40 mM) cyanide, top; + saturating azide (40 mM), middle; and anion-free Mn(III)/Mn(IV) catalase, bottom. All solutions were prepared in sodium phosphate with a nominal (room temperature) pH of 7 (see text). Simulations used parameters given in Table 3.

Table 3. EPR Spectral Simulation Parameters

simulation parameters[a]	Mn catalase	Mn catalase + 20 mM N_3^-	Mn catalase + 40 mM CN^-
line width ($W_{\|\|}$)[b]	1.09	0.802	0.802
line width ($W_\perp$)[b]	1.31	1.10	1.10
$g_{\|\|}$	1.994	1.994	1.994
$g_\perp$	2.009	2.008	2.008
$A_{Mn(III)_{\|\|}}$[c]	104	101	98.1
$A_{Mn(III)_\perp}$[c]	142	137	137
$A_{Mn(IV)_{\|\|}}$[c]	83.2	81.8	78.9
$A_{Mn(IV)_\perp}$[c]	75.2	74.6	72.5

[a] Spectra simulated for axially symmetric systems. Simulations using rhombic parameters gave comparable fits. [b] Linewidth in mT. [c] Hyperfine coupling constants in units of $cm^{-1} \times 10^4$.

Mn catalase.[48] However, addition of F^- up to 100 mM (at pH 7.0) caused no perturbation in the EPR spectrum.

The EPR spectra for the azide- and cyanide-treated samples were simulated in order to quantitate the observed changes. As with the untreated superoxidized catalase, all spectra were adequately simulated using an axially symmetric Hamiltonian.[35] The experimental and simulated spectra for all three superoxidized derivatives are compared in Figure 6, and the simulation parameters are given in Table 3.

ESEEM Spectroscopy. Figure 7 shows the time domain (A) and frequency domain (B) 3-pulse ESEEM spectra for the azide-free and azide-treated catalase obtained at X- and P-band microwave frequencies. The X-band data obtained at a field value of 391.0 mT for the azide-free sample shows a classic "exact cancellation" ^{14}N ESEEM pattern, with three sharp low-frequency transitions (at 0.66, 1.39, and 2.03 MHz) and a broader transition at higher frequency (5.8 MHz). This exact cancellation occurs when the magnitudes of the applied magnetic field and the ^{14}N superhyperfine field are closely matched.[40,49,50] In this case, the applied and superhyperfine fields cancel for one-electron spin orientation, and the ^{14}N ESEEM frequencies

(48) Stemmler, T. L.; Blazyk, J. L.; Sharma, Y. K.; Roy, A.; Waldo, G. S.; Arulsamy, N.; Goff, H.; Penner-Hahn, J. E., unpublished results.

(49) Flanagan, H. L.; Singel, D. J. *J. Chem. Phys.* **1987**, *87*, 5606−5616.

(50) Mims, W. B.; Peisach, J. *J. Chem. Phys.* **1978**, *69*, 4921−4930.

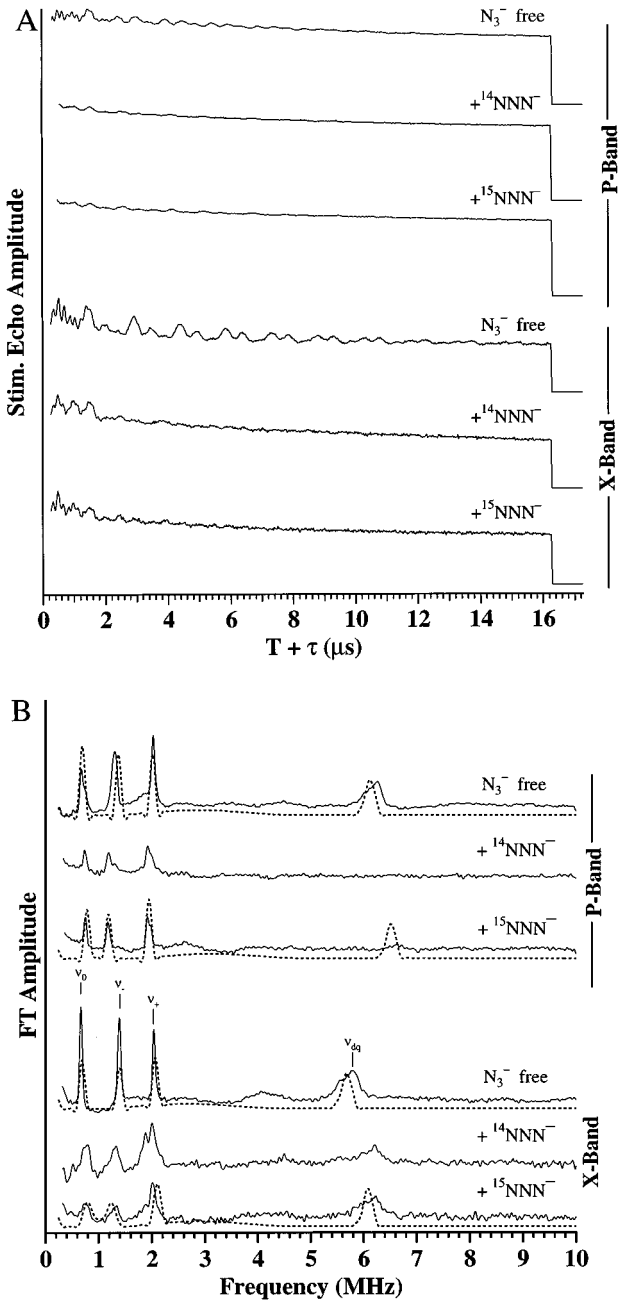

Figure 7. Multifrequency ESEEM spectra for superoxidized catalase ± ^{14}N and ^{15}N azide (pH 7.0 in 50 mM phosphate buffer, $[N_3^-] = 160$ mM). (A) Multifrequency 3-pulsed ESEEM time domain pattern of azide-free and azide-treated catalase. The long length of time over which the modulation occurs in the absence of azide at X-band is typical of exact-cancellation conditions. (B) Frequency domain ESEEM spectra of azide-free and azide-treated superoxidized catalase obtained by Fourier analysis of time domain traces from panel A. The NQR transitions (ν_0, ν_-, and ν_+) and the double quantum transition (ν_{dq}) are indicated. Dashed lines are simulations using NQR and hyperfine parameters listed in Table 4. Experimental parameters were repetition rate = 200 Hz, $\pi/2$ pulse width = 15 ns, microwave power ≈ 10 W. P-band: ν_{MW} = 13.098 GHz (N_3^--free), 12.980 GHz (NNN$^-$), and 13.206 GHz (^{15}NNN$^-$); B = 477.1 mT (N_3^--free), 474.8 mT (NNN$^-$), and 483.5 mT (^{15}NNN$^-$); and τ = 197 ns (N_3^--free), 200 ns (NNN$^-$), and 196 ns (^{15}NNN$^-$). X-band: ν_{MW} = 10.995 GHz; B = 400.2 mT; τ = 176 ns.

arise solely from the nuclear quadrupole interactions. The three low-frequency transitions in this spin manifold correspond to the zero field nuclear quadrupole resonance (NQR) transitions ν_0, ν_-, and ν_+. These frequencies are related to the ^{14}N nuclear quadrupole parameters e^2qQ and η by eq 2:

$$\nu_+ = \frac{1}{4}(3+\eta)e^2qQ$$

$$\nu_- = \frac{1}{4}(3-\eta)e^2qQ \qquad (2)$$

$$\nu_0 = \frac{1}{2}\eta e^2qQ$$

The lack of "combination lines" that would result from modulation from multiple ^{14}N nuclei indicates that a single ^{14}N is the source of the observed modulation.[51] The other electron spin orientation results in the addition of applied and superhyperfine fields, leading to a "double quantum" ^{14}N spin transition between the outermost energy levels of this manifold. For azide-free catalase, this is observed at 5.8 MHz. In the approximation that the superhyperfine coupling is isotropic with a coupling constant A, the frequency of the double quantum transition is given by eq 3,

$$\nu_{dq} = 2\left[\left(\nu_i + \frac{1}{2}|A|\right)^2 + \frac{(e^2qQ)^2}{16}(3+\eta^2)\right]^{1/2} \qquad (3)$$

where ν_i is the ^{14}N Zeeman frequency. The two "single quantum" ^{14}N spin transitions (i.e., those between the two outer energy levels and the inner level) of this "non-cancelled" manifold are typically too broad to be observed in the ESEEM experiments with a non-zero dead time. Use of eqs 2 and 3 provides a convenient starting point for ESEEM simulations. The dashed line in Figure 7B shows the frequency domain simulation using a quadrupolar coupling value of $e^2qQ = 2.19$ MHz, $\eta = 0.58$, and an A value of 2.88 MHz (Table 4). A dipolar hyperfine component of −0.1 MHz was also included in the simulation in addition to the isotropic A value. The simulation shows good frequency matches to the three NQR peaks and the double quantum peak.

Upon addition of azide, the ^{14}N NQR peaks broaden considerably but remain in approximately the same positions. The double quantum peak shifts up in frequency to 6.2 MHz, corresponding to an increase in the superhyperfine coupling. Since the NQR frequencies are unchanged relative to the azide-free protein, it seems likely that these ^{14}N transitions are due to the same protein nitrogen as seen in the azide-free sample. Experiments performed with terminally ^{15}N-labeled azide (^{15}NNN$^-$) are consistent with this assignment. The peak amplitudes and positions are essentially unchanged with this isotope substitution (there is some diminution in a secondary feature at 1.88 MHz), indicating that the major modulation features observed in the azide-treated sample are not due to the terminal nitrogens of azide.

The increased superhyperfine coupling that is induced by azide treatment shifts the double quantum feature to higher frequency. This suggests that a better-resolved ESEEM spectrum for the azide-treated sample could be obtained by working at a higher magnetic field. Indeed, the P-band data obtained at higher fields show a dramatic sharpening of the ^{14}N NQR peaks in the azide-treated sample. The NQR frequency values of 0.79, 1.17, and 1.93 MHz and the double quantum frequency of 6.61 MHz for the azide-treated sample (seen better in 2-pulse data, not shown) are simulated well with ^{14}N spin Hamiltonian parameters of $e^2qQ = 1.97$ MHz, $\eta = 0.74$, and $A = 3.34$ MHz (Table 4).[52] These same simulation parameters also reproduce

(51) McCracken, J.; Pember, S.; Benkovic, S. J.; Villafranca, J. J.; Miller, R. J.; Peisach, J. *J. Am. Chem. Soc.* **1988**, *110*, 1069−1074.

Table 4. ^{14}N Spin Hamiltonian Parameters for Superoxidized Manganese Catalase

sample	$A_{^{14}N}$(MHz)	e^2qQ (MHz)[a]	η
native	2.88	2.19	0.58
native + N_3^-	3.34	1.97	0.74
native + CN^-	3.86	1.93	0.74

[a] Estimated uncertainty in e^2qQ is ±0.05 MHz.

the broadening and shifting of the features in the X-band data upon azide incubation. Similarly, the simulation parameters used previously to simulate the X-band spectra of the untreated sample give good simulations of the P-band spectra of the untreated sample.

Since we were able to obtain neither fully labeled azide nor azide ^{15}N-labeled at the central nitrogen position, the possibility remains that the ^{14}N ESEEM features in the azide-treated sample could result from the central azide nitrogen. This motivated us to perform ESEEM experiments with $C^{14}N^-$ and $C^{15}N^-$. The X-band ESEEM spectra (Figure 8) following cyanide treatment shows a broadening of features in the NQR region and an upshift of the double quantum frequency. Because conversion to the cyanide-altered form of the catalase EPR signal was incomplete at the cyanide concentration used in the ESEEM experiment (120 mM), weak transitions from the cyanide-free enzyme are still observed (marked with § in Figure 8). However, no ESEEM differences are observed in the cyanide-treated samples using the two nitrogen isotopes. Thus it is clear that all of the ^{14}N modulation results from protein nitrogen. Similarly to the azide-treated sample, the cyanide-treated sample gives rise to spectra with better resolution at the higher field used for P-band microwave excitation (only $C^{14}N^-$ data were recorded at the higher frequency). Spin Hamiltonian values used in the simulations of the ESEEM spectra for the cyanide-treated samples are $e^2qQ = 1.93$ MHz, $\eta = 0.74$, and $A = 3.86$ MHz (Table 4).

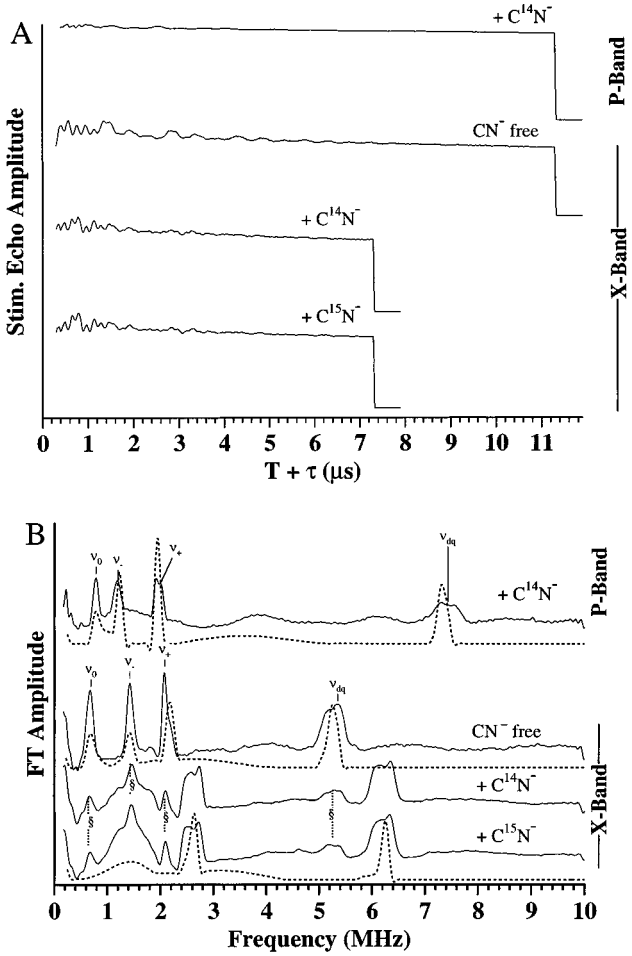

Figure 8. Multifrequency ESEEM spectra for superoxidized catalase ± ^{14}N and ^{15}N cyanide (pH 7.0 in 50 mM phosphate buffer, $[CN^-]$ = 120 mM). (A) Multifrequency 3-pulsed ESEEM time domain patterns for cyanide-free and cyanide-treated catalase. (B) Frequency domain ESEEM spectra obtained by Fourier analysis of the time domain traces from panel A. The NQR transitions (ν_0, ν_-, and ν_+) and the double quantum transition (ν_{dq}) are indicated. Dashed lines are simulations using NQR and hyperfine parameters listed in Table 4. The cyanide treatment led to incomplete conversion and a fraction of cyanide-free catalase remains. Features due to cyanide-free catalase are marked with §. Experimental parameters were repetition rate = 200 Hz, $\pi/2$ pulse width = 15 ns, microwave power ≈ 10 W. P-band: ν_{MW}, = 13.718 GHz; B = 528.9 mT ; τ = 222 ns. X-band: ν_{MW}, = 9.2774 GHz; B = 331.1 mT ; τ = 213 ns.

Discussion

Structure of the Mn Site. The similarity of the XAS spectra in the presence and absence of azide suggests that azide binding causes, at most, small changes in either the geometry or the Mn ligation. The similarity of the XANES spectra and the absence of any significant decrease in the 1s → 3d intensity in the presence of azide suggest that azide binding does not cause a change in coordination number.[29,53] This could indicate either that azide binds to Mn with concomitant displacement of another ligand or that azide does not bind directly to the Mn. The EXAFS data provide further evidence that the basic $Mn_2(\mu\text{-}O)_2$ core structure is perturbed only slightly by the addition of azide. Although the appearance of features in the Fourier transform change fairly significantly following azide addition, this is a consequence of the Fourier transformation and not an indication of significant structural change, as shown by the similarity of the refined structural parameters.

The Mn···Mn distance increases from 2.70 to 2.73 Å on addition of azide. In crystallographically characterized $Mn^{III}(\mu\text{-}O)_2Mn^{IV}$ structures, Mn···Mn distances vary from ca. 2.65 to 2.75 Å.[44] Typically, the shorter distances (<2.70 Å) are found for dimers that have an additional bridging ligand, such as a carboxylate, while the longer distances are characteristic of unsupported $(\mu\text{-}O)_2$-bridged dimers. On this basis, we had previously suggested that superoxidized catalase might have a $Mn(\mu\text{-}O)_2(\mu\text{-}CO_2)Mn$ structure.[14] With the improved distance calibration of the present data, the support for this conclusion is less clear cut. The current Mn···Mn distances would be consistent with either a $Mn(\mu\text{-}O)_2Mn$ or a $Mn(\mu\text{-}O)_2(\mu$-carboxylate) Mn core structure.

One interpretation of the increase in Mn···Mn distance on azide binding would be that azide displaces a carboxylate bridge (e.g., converting μ-1,3 bridging carboxylate into a monodentate carboxylate). A recent combined UV−visible/MCD study[19] suggests another explanation for the change in distance. In this work, the oxo → Mn charge transfer transitions were found to be unusually weak, suggesting relatively poor oxo−Mn orbital overlap. This was interpreted in terms of a $Mn(\mu\text{-}O)_2Mn$ core that was slightly bent along the O−O axis. The absorption intensity increased on addition of azide, suggesting that the $Mn(\mu\text{-}O)_2Mn$ core flattens slightly in the presence of azide. A flattening of the core by 5−10° would account for the ca. 0.03

(52) The double quantum peak is broadened significantly beyond that observed in the simulation. This effect may result from increased inhomogeneity in the hyperfine interaction upon azide inhibition.

(53) Randall, C. R.; Shu, L.; Chiou, Y. M.; Hagen, K. S.; Ito, M.; Kitajima, N.; Lachicotte, R. J.; Zang, Y.; Que, L. J. *Inorg. Chem.* **1995**, *34*, 1036−1039.

Å increase in the Mn···Mn distance when azide is added. This flattening could be the result of loss of a carboxylate bridge, or it could reflect a protein-induced conformational change.

The EXAFS data for superoxidized catalase show evidence for outer shell scattering typical of imidazole ligation.[24,54] The apparent average coordination number for the 4.3 Å shell is ca. two carbons per Mn, suggesting a lower limit of two imidazoles coordinated per Mn dimer. The apparent coordination number for the ca. 3.0 Å shell is somewhat larger. This is probably due to additional contributions from other, non-imidazole carbons. Using the known geometry of the imidazole ring in hexakisimidazole Mn(II) dichloride, the observed N_3/C_4 distance of ca. 4.30 Å implies Mn···C_2/C_5 and Mn−N_1 distances of 3.15 and 2.14 Å, respectively. This calculated Mn···C_2/C_5 distance is substantially longer than the apparent Mn···C_2/C_5 distance (ca. 3.0 Å) seen in the EXAFS, probably reflecting the presence of additional scatters at ∼3.0 Å in superoxidized catalase. Scattering from monodentate and bidentate 1,3-bridging carboxylates is expected to occur in this range[55−57] and could account for both the the lower-than-expected Mn···C_2/C_5 distances and the larger-than-expected Mn···C_2/C_5 coordination numbers found in Table 2. The calculated Mn−N_1 distance is consistent with the Mn−O/N average bond length found by EXAFS curve fitting (2.05−2.09 Å), since the EXAFS distance is undoubtedly the average of a range of shorter Mn−O and longer Mn−N distances.

In the presence of azide, there is a slight decrease in the amplitude of the Mn···N_3/C_4 scattering, as seen by the slightly lower apparent coordination number and by the fact that the corresponding peak in the Fourier transform (Figure 2) is at or only slightly above the noise level of the data. One explanation for this decrease would be the loss of an imidazole ligand when azide binds. A more likely explanation for the decrease in N_3/C_4 amplitude in the azide-treated sample is an increase in the disorder of the imidazole shells. In particular, the N_3/C_4 scattering is very sensitive to the Mn−N_1−C_5 angle, as a result of multiple scattering. On the basis of FEFF simulations, a rotation as small as 5−10° in one of the imidazoles would be sufficient to account for the change in the amplitude of the Mn···N_3/C_4 peak.[24]

Titrations with Azide and Cyanide. Addition of either azide or cyanide causes reversible changes in the UV−visible and EPR spectra. The changes in the UV−visible spectra involve an increase in the intensity of all of the transitions. These changes are not due simply to chaotropic effects, since comparable concentrations of F^-, Cl^-, or phosphate do not cause similar spectral perturbations. The EPR spectra show resolvable features corresponding to two limiting forms of the enzyme. Spectra measured at intermediate azide or cyanide concentrations show resolved contributions from both of the limiting forms (this is most easily seen on the low- and high-field transitions), thus demonstrating that this behavior is best described as equilibrium binding of azide and cyanide to superoxidized catalase.

The titrations show that anion binding is pH dependent, with tighter anion binding at lower pH. At pH 7.0, the $[N_3^-]_{1/2}$ determined by UV−visible spectroscopy is ca. 18 mM. In contrast, the EPR titration at this pH gives an apparent $[N_3^-]_{1/2}$ of 40 mM. This difference may reflect a temperature dependent equilibrium constant. The absence of any perturbations in the EPR spectrum for azide concentrations up to 150 mM at pH 8.5 demonstrates that $[N_3^-]_{1/2}$ under these conditions must be greater than ca. 500 mM, while the observation of $[N_3^-]_{1/2} \approx 5$ mM at pH 5.5 is consistent with stronger azide binding at lower pH. The pH dependence of $[N_3^-]_{1/2}$ could be due either to the binding of protonated anions (HCN has a pK_a of 9.31; HN_3 has a pK_a of 4.72)[58] or to the requirement for protonation of a site on the enzyme prior to anion binding. In the absence of azide or cyanide, no pH dependence is observed for the EPR spectra of superoxidized catalase from pH 5.5 to 8.5 (data not shown).

It was not possible to determine an accurate $[CN^-]_{1/2}$ at pH 7.0, due to protein precipitation. From the UV−visible spectra, it is clear that cyanide binds less strongly than azide. From the EPR-determined $[CN^-]_{1/2}$ at pH 5.5, the binding of cyanide is ca. 5 times weaker than that of azide under comparable conditions. If this ratio holds at pH 7.0, $[CN^-]_{1/2}$ should be ca. 65 mM, which would be consistent with the observed UV−visible spectra.

The binding data (Figure 3 and supplementary material) provide clear evidence for cooperative anion binding, but are not sufficient to distinguish between possible models of cooperativity. One possible mechanism for cooperativity would be an anion-induced change in the Mn core structure, as suggested by the spectroscopic data (see below).

Effect of Azide and Cyanide on the Mn Site. The binding of azide or cyanide causes no significant change in the energies of the UV−visible transitions, but results in increased intensities. This is consistent with the earlier observation that azide binding resulted in an increase in UV−visible intensity but had no effect on the energies of the UV−visible or MCD features.[19] These changes are consistent with the presence of a slightly bent Mn(μ-O)$_2$Mn core in the absence of anions and a flatter core following binding of azide or cyanide. A flatter Mn(μ-O)$_2$Mn core results in better overlap between the oxo 2p and Mn 3d orbitals, causing an increase in charge-transfer intensity and possibly accounting for the changes in the 1s → 3d region. The absence of any significant changes in the UV−visible transition energies suggests that there are no major changes in Mn ligation when azide or cyanide bind.

The EPR perturbations are consistent with this structural picture. The binding of azide and cyanide causes no significant changes in the *g* values or in the *A* anisotropy. The only significant changes that occur on binding azide and cyanide are an approximately 20% decrease in line width and a very slight (3−4%) decrease in ^{55}Mn hyperfine coupling. The two anions have nearly identical effects on *A*, with CN^- giving a slightly greater decrease. A decrease in the ^{55}Mn hyperfine coupling is consistent with a flatter Mn(μ-O)$_2$Mn core, since this should lead to slightly greater spin delocalization onto the oxo bridges. The two hyperfine coupling tensors show nearly identical decreases, providing additional evidence that the anion-induced changes are not localized on either the Mn(III) or the Mn(IV) ion. Given these observations and given the nearly identical behavior of azide and cyanide, it is unlikely that either anion is coordinated *directly* to the Mn site.

ESEEM Spectroscopy. The ESEEM results for isotopically labeled azide and cyanide demonstrate that the observed ESE modulation in the anion-treated samples arises from protein-derived ligands. The ^{14}N quadrupolar parameters are similar in all cases, so it is likely that the same protein nitrogen gives rise to the modulation in all three samples, with slight changes

(54) Stemmler, T. L. Ph.D. Thesis, The University of Michigan, 1996.
(55) Wieghardt, K.; Bossek, U.; Zsolnai, L.; Huttner, G.; Blondin, G.; Girerd, J. J.; Babonneau, F. *J. Chem. Soc., Chem. Commun.* **1987**, 651−653.
(56) Pal, S.; Armstrong, W. H. *Inorg. Chem.* **1992**, *31*, 5417−5423.
(57) Sheats, J. E.; Czernuszewicz, R. S.; Dismukes, G. C.; Rheingold, A. L.; Petrouleas, V.; Stubbe, J.; Armstrong, W. H.; Beer, R. H.; Lippard, S. J. *J. Am. Chem. Soc.* **1987**, *109*, 1435−1444.
(58) *The Merck Index*, 11th ed.; Budavari, S., O'Neil, M. J., Smith, A., Heckelman, P. E., Eds.; Merck & Co.: Rahway, NJ, 1989.

due to small perturbations in the cluster ligand geometry. The lack of modulation from azide is a strong indicator that azide does not bind directly to Mn. Although it is possible that a directly bound nitrogen could have a superhyperfine interaction too strong to give rise to appreciable modulation (vide infra), it is very unlikely that all three of the chemically inequivalent nitrogens would be in such a strongly coupled limit.

Our *L. plantarum* catalase ESEEM results are somewhat comparable to those of Dikanov et al.[59] for the *T. thermophilus* enzyme ($e^2qQ = 2.44$ MHz, $\eta = 0.44$, and $A = 2.3$ MHz). Dikanov et al. attributed the modulation to a remote nitrogen of a coordinating histidine, such as observed in a variety of Cu(II) enzymes.[60] However, more recent studies of Mn(III)/Mn(IV) model compounds do not support this interpretation.[61−65] For example, strong ^{14}N ESEEM features are seen for each member of a series of seven distinct Mn(III)/Mn(IV) clusters with nitrogens directly coordinated to Mn.[63,64] No noncoordinated nitrogens are present in any of these compounds. The range of superhyperfine couplings for these compounds is 2.51−3.04 MHz. In analysis of the model compound data, the ESEEM-detected nitrogens are assigned to those bound to the Mn(IV) ions of the various mixed valence pairs.[66] The 2.88 MHz coupling for the ESEEM-detected nitrogen in superoxidized catalase is squarely in this range, leaving little doubt that it arises from a direct ligand to the Mn(III)/Mn(IV) core, and most likely from a nitrogen coordinated to the Mn(IV) ion.

The ^{14}N superhyperfine coupling increases in the anion-treated samples (3.34 MHz for azide and 3.86 MHz for cyanide). This is consistent with the decrease in ^{55}Mn hyperfine couplings for both Mn(III) and Mn(IV) ions that is seen in the EPR. Each anion thus decreases the unpaired spin density on both of the Mn ions and increases it on at least one of the ligands. This may be another result of the core flattening discussed earlier.

The chemical identity of the nitrogen that is seen by ESEEM remains uncertain. The EXAFS spectra are best fit with approximately two histidine ligands (i.e., one histidine per Mn), so it is appealing to assign the ESEEM spectral features to the ligated nitrogen of a bound histidine. Continuous wave ENDOR experiments on the *T. thermophilus* enzyme failed to detect nitrogen transitions and were therefore inconclusive as to the nature of nitrogen ligation to the Mn_2 cluster.[67] A recent ESEEM study of the N_3^-/CN^--free *T. thermophilus* enzyme gave ^{14}N parameters of $e^2qQ = 2.34$ MHz, $\eta = 0.51$, and $A = 2.45$ MHz.[61] The ESEEM pattern was altered dramatically by a reductive methylation treatment which resulted in methylation of 64% of the lysine residues but only 3% of the histidine residues. This result, along with a "fingerprint" comparison of the N_3^-/CN^--free catalase ESEEM to the ESEEM of ammonia bound to the OEC Mn cluster,[40] was used to argue for the presence of a lysine bridge in superoxidized catalase. While the "fingerprint" may be consistent with a lysine bridge, it is also consistent with a coordinated imidazole. The e^2qQ values

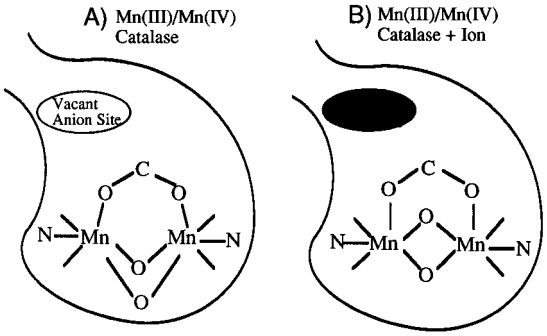

Figure 9. Proposed azide and cyanide binding site and perturbation of Mn core upon ion binding. (A) Mn(III)/Mn(IV) catalase with vacant ion site, consistent with a bent Mn(III)/Mn(IV)(μ-oxo)$_2$(μ-RCO$_2$) core. (B) More nearly planar Mn(III)/Mn(IV)(μ-oxo)$_2$(μ-RCO$_2$) core of superoxidized enzyme upon binding of azide or cyanide. The two imidazole ligands identified from the EXAFS are indicated by N, with one coordinated to each Mn, as suggested by the ESEEM. No geometric information is implied by the placement of the N ligands. The remaining 2−3 ligands per Mn, presumably carboxylates and/or solvent molecules, are indicated by lines. On the basis of the pH dependence of anion binding, either the anion or the binding site must be protonated for strong anion binding.

for Mn catalase (2.29 MHz for *L. plantarum*; 2.34 or 2.44 MHz for *T. thermophilus*) are in the center of the 1.9−2.8 MHz range found by Ashby et al.[68] in NQR studies of metal coordinated imino nitrogens in a series of metal−imidazole complexes. Since azide and cyanide shift the ligand superhyperfine couplings even though they do not appear to bind directly to the cluster, it is easily conceivable that the harsh methylation treatment performed on the *T. thermophilus* enzyme alters the protein structure sufficiently to cause the observed changes in the ESEEM spectrum. For example, methylation of a lysine near the Mn site rather than disruption of a lysine bridge might be responsible for the changes in the ESEEM spectra. At this point, we feel that the combination of EXAFS and ESEEM data argues most strongly for histidine ligation, but does not rule out other possibilities. ESEEM experiments using selectively labeled [^{15}N]histidine[69] should resolve this question and are in progress.

The EXAFS data suggest coordination of two histidine ligands to the Mn_2 core, while the ESEEM experiment detects only one bound nitrogen, most likely the directly bound nitrogen of a histidine ligand to the Mn(IV) ion. It is possible that a second histidine ligand binds at a site where the superhyperfine coupling is too strong to be observed via ESEEM at the high-field values employed to date. ENDOR experiments have shown nitrogen superhyperfine couplings of $A \approx 10$ MHz in some nitrogen-coordinated Mn(III)/Mn(IV) complexes.[63,66,67,70] These more strongly coupled nitrogens are likely to be those that are coordinated along the Jahn−Teller axes of the Mn(III) ions, because these nitrogens should have the most unpaired spin density due to their overlap with the half-filled d_{z^2} orbital. Similar histidine coordination in the catalase enzyme would be likely to give superhyperfine coupling that is too large to be easily detected in our ESEEM experiments. Recent analysis of the ESEEM and ENDOR data for Mn(III)/Mn(IV) model compounds[66] suggests that the hyperfine tensors of the equatorially bound nitrogen ligands of the Mn(III) ions are highly anisotropic and may be difficult to observe with either ESEEM or ENDOR. It is possible that the broad features observed in

(59) Dikanov, S. A.; Tsuetkov, Y. D.; Khangulov, S. V.; Goldfeld, M. G. *Dokl. Akad. Nauk SSSR* **1988**, *302*, 1255−7.
(60) Mims, W. B.; Peisach, J. *Biological Magnetic Resonance*; Plenum: New York, 1981; Vol. 3, pp 213−263.
(61) Ivancich, A.; Barynin, V. V.; Zimmermann, J. L. *Biochemistry* **1995**, *34*, 6628−6639.
(62) Britt, R. D. Thesis, University of California, Berkeley, 1988.
(63) Britt, R. D.; Sturgeon, B. A.; Randall, D. W.; Chan, M. K.; Klein, M. P.; Armstrong, W. H., unpublished results.
(64) Sturgeon, B. E. Thesis, Department of Chemistry, University of California (Davis), 1994.
(65) Britt, R. D.; Klein, M. P. In *Pulsed Magnetic Resonance: NMR, ESR, and Optics, a Recognition of E. L. Hahn*; Bagguley, D. M. S., Ed.; Clarendon: Oxford, 1992; pp 361−376.
(66) Randall, D. W. Ph.D. Thesis, University of California, 1997.
(67) Khangulov, S.; Sivaraja, M.; Barynin, V. V.; Dismukes, G. C. *Biochemistry* **1993**, *32*, 4912−4924.
(68) Ashby, C. I. H.; Cheng, C. P.; Brown, T. L. *J. Am. Chem. Soc.* **1978**, *100*, 6057−6067.
(69) Tang, X. S.; Diner, B. A.; Larsen, B. S.; Gilchrist, M. L.; Lorigan, G. A.; Britt, R. D. *Proc. Natl. Acad. Sci. U.S.A.* **1994**, *91*, 704−708.
(70) Tan, X. L.; Gultneh, Y.; Sarneski, J. E.; Scholes, C. P. *J. Am. Chem. Soc.* **1991**, *113*, 7853−7858.

the 4−5 MHz range of the frequency-domain ESEEM spectra (see Figures 7B and 8B) arise from such coupled nitrogens. Therefore, our favored assignment, based on the combined EXAFS and ESEEM data, is that there is a single histidine coordinated to each of the two Mn ions in the mixed valence core.

Relationship to Active Catalase. The superoxidized derivative of Mn catalase is inactive, and thus anion interactions with the superoxidized enzyme are not necessarily catalytically relevant. However, there are striking parallels between interactions of azide and cyanide with superoxidized catalase and with active catalase. Kinetic studies have shown that azide and cyanide interact with active Mn catalase, and, in particular, that azide is a competitive inhibitor of Mn catalase.[16] NMR relaxation measurements have shown that azide blocks solvent exchange to the Mn in the reduced enzyme.[16] In both cases, azide binds substantially more tightly than cyanide, and both anions bind in a pH dependent manner, with stronger binding at low pH. Finally, the values of $[N_3^-]_{1/2}$ for the reduced and the superoxidized catalase are the same within 1 order of magnitude.

These observations would be consistent with azide binding to a similar site in both the superoxidized and the reduced derivatives of the enzyme. For the superoxidized enzyme, the present data show that the azide binding site is on the protein and not on the Mn, although presumably the azide binding site is sufficiently close to the Mn that it can perturb the Mn geometry (see Figure 9). If azide binds at the same site in the active enzyme as it does in the superoxidized enzyme, then the observation that azide is a competitive inhibitor would imply that peroxide binding to this protein-based site is an essential step in the catalytic mechanism. The structural perturbations that are caused by anion binding may thus be important in controlling the reactivity of the binuclear Mn unit.

Conclusions

The binding of azide or cyanide causes small perturbations in the structural and electronic properties of the Mn(III)(μ-O)$_2$Mn(IV) site in Mn catalase but no significant change in the basic core structure. EXAFS data suggests that there are two His residues coordinated to the Mn_2 core, one of which is detectable in X-band ESEEM spectra. There are no ESEEM detectable features attributable to direct coordination of the azide or cyanide anions to the Mn_2 core. These observations point to the existence of a protein-based anion binding site which may be important in the catalytic mechanism of Mn catalase.

There is substantial interest in understanding the EPR properties of the OEC. The present data demonstrate that significant changes in Mn hyperfine coupling can occur as the result of apparently minor changes in geometry and in the absence of large changes in ligation. Similar minor structural variations may be responsible for the changes in the number of resolvable lines in the OEC EPR spectra when, for example, Ca is depleted or replaced by Sr or when NH_3 binds.[6]

Acknowledgment. This work was supported in part by grants from the NIH (GM-45205 to J.E.P.-H.; GM-48242 to R.D.B.). SSRL and NSLS are supported by the U.S. Department of Energy with additional support from the NIH Research Resource program. Beamline X-19A was supported in part by the University of Michigan Office of the Vice President for Research. The authors thank Alice Haddy for helpful discussions and acknowledge Geoff Waldo for his original work with the ESEEM data collection.

Supporting Information Available: EPR-detected titrations with N_3^- and CN^- (3 pages). See any current masthead page for ordering and Internet access instructions.

JA9704040